Applied Catalysis B: Environmental 119–120 (2012) 100–108

Contents lists available at SciVerse ScienceDirect

Applied Catalysis B: Environmental

journal homepage: www.elsevier.com/locate/apcatb

The effect of the morphological characteristics of TiO_2 supports on the reverse water–gas shift reaction over Pt/TiO_2 catalysts

Sung Su Kim, Hyun Hee Lee, Sung Chang Hong*

Department of Environmental Energy Systems Engineering, Graduate School of Kyonggi University, 94-6 San, Iui-dong, Youngtong-ku, Suwon-si, Gyeonggi-do 442-760, Republic of Korea

ARTICLE INFO

Article history:
Received 16 September 2011
Received in revised form 20 February 2012
Accepted 22 February 2012
Available online 2 March 2012

Keywords:
Pt
TiO_2
CO_2
RWGS
SMSI

ABSTRACT

The effect of the morphological characteristics of a TiO_2 support on the reverse water–gas shift reaction over Pt/TiO_2 catalysts was examined. The activity of Pt catalysts with 6 different types of TiO_2 supports varied during the reverse water–gas shift reaction. Analysis using H_2 Temperature Programmed Reduction (TPR) and Temperature Programmed Desorption (TPD) confirmed that the active sites of the Pt/TiO_2 catalyst included both the Pt sites and the TiO_2 sites, which were reducible, and the difference in the activity of the Pt/TiO_2 catalysts was dependent on the reducibility of the TiO_2 supports. X-ray diffraction (XRD) analysis showed that the TiO_2 crystallite size was a key factor that dictated the reducibility of the TiO_2 sites.

1. Introduction

Carbon dioxide is one of the major causes of global warming. The CO_2 concentration in the atmosphere significantly increased through the increased use of fossil fuels, which has strongly affected both the global weather and the ecosystem and could cause considerable damage to mankind.

Currently, carbon dioxide utilization is being evaluated using heterogeneous catalysis with the goal of decreasing the effects of global warming. Heterogeneous catalysis has several technical advantages, including high system stability, effective separation of products, easy operation, the ability to reuse the catalysts and simple reactor design [1]. Heterogeneous catalysis can be used for the hydrogenation of CO_2, which can produce energy sources, such as CO, CH_4 and methanol or the raw material of C1 chemistry through the reaction of CO_2 with hydrogen. Recently, Wang et al. [2] examined RWGS, CO_2 methanation, MeOH, hydrocarbon, formic acid, formates, formamides and dimethyl ether (DME) synthesis, which involve the catalytic hydrogenation of CO_2. DME synthesis combines the dehydration process during the synthesis process for the formation of methanol, whereas the hydrocarbon synthesis process involves the combination of the RWGS process and the Fischer–Tropsch process. In addition, the synthesis of formic acid, formates and formamides utilizes homogeneous catalysis. Therefore, the foundation hydrogenation reactions using heterogeneous catalysis involve the reactions shown below:

$$H_2 + CO_2 \rightarrow CO + H_2O \text{(Reverse water–gas shift reaction)} \quad (1)$$

$$4H_2 + CO_2 \rightarrow CH_4 + 2H_2O \text{(Methanation)} \quad (2)$$

$$3H_2 + CO_2 \rightarrow CH_3OH + H_2O \text{(MeOH synthesis)} \quad (3)$$

Methanation has some shortcomings, including a large consumption of hydrogen in the reaction and difficulties in transporting and storing the product, methane. The synthesis of methanol is difficult because the conversion rate for the direct reaction between carbon dioxide and hydrogen is low. In contrast, the RWGS reaction has many advantages, including low hydrogen consumption (1 mol), a high equilibrium conversion rate and the fact that the CO product can be used as the main raw material for C1 chemistry. Recently, Park et al. [3] utilized the CAMERE (carbon dioxide hydrogenation to form methanol via a reverse water–gas shift reaction) process, which was associated with the RWGS reaction, for MeOH synthesis; the authors proposed that the RWGS reaction can be used to directly reduce carbon dioxide.

There have been many previous studies on RWGS reactions. With regard to studies using transition-metal catalysts, Chen et al. [4] and Luhui et al. [5] have studied the RWGS reaction using Ni/CeO_2 and Cu/SiO_2; however, these catalysts showed poor performance and selectivity. Wang et al. [2] reported that the 2% Ni/CeO_2 catalyst showed excellent catalytic activity and stability during the RWGS reaction. According to this previous study, oxygen vacancies in the CeO_2 lattice and dispersed Ni sites are the main active

* Corresponding author. Tel.: +82 31 249 9744; fax: +82 31 254 4905.
E-mail address: schong@kyonggi.ac.kr (S.C. Hong).

0926-3373/$ – see front matter © 2012 Elsevier B.V. All rights reserved.
doi:10.1016/j.apcatb.2012.02.023

site for RWGS. Liu and Liu [6] also examined a series of bimetallic Cu–Ni/Al_2O_3 catalysts for CO_2 hydrogenation. They reported that the ratio of Cu/Ni significantly affects the conversion and selectivity. Except for these studies, most studies have evaluated the generation of CO in the methanation reaction using catalysts with poor CH_4 selectivity. In contrast, Park et al. [3] reported that catalysts that contained Zn and Al_2O_3 performed well in the RWGS reaction. According to this previous study, the $ZnAl_2O_4$ catalyst prepared at a temperature of 850 °C or higher showed the highest performance and selectivity, and catalysts calcined at lower temperatures were not stable due to the evaporation of active metal, Zn.

Many studies have examined the use of the Pt catalyst, a noble metal in the WGS (water–gas shift reaction), which is the reverse reaction of the RWGS [7–10]. The reactions using Pt/TiO_2, Pt/CeO_2 and Pt/CeO_2–TiO_2 catalysts, which have been shown to strongly interact with the metal support, have been shown to exhibit the best performance. In contrast, few studies have evaluated the potential of using Pt catalysts in RWGS reactions. However, recently, Goguet et al. [11] examined the mechanism and intermediates of the RWGS reactions using the Pt/CeO_2 catalyst. They claimed that the support site, which can be reduced, functioned as the main active site in the RWGS reaction. Pekridis et al. [12] also examined the electrokinetics of the RWGS reaction over Pt in a solid-oxide fuel cell.

TiO_2 can be reduced and has been shown to produce the SMSI effect with Pt. The SMSI effect, which is caused by the strong interaction between reduced Ti^{3+} sites and Pt, can produce reduction sites on a TiO_2 support. Therefore, TiO_2 is expected to be suitable support for catalysts and to improve the performance of the catalyst in the RWGS reaction. Therefore, in this study, the physical and chemical properties of Pt/TiO_2 catalysts using various commercial TiO_2 catalysts with different properties were examined, and the factors that affected the catalytic activity were determined.

2. Experimental methods

2.1. Catalyst preparation

The Pt/TiO_2 catalysts were prepared using the impregnation method [13]. $PtCl_4$ was purchased from Sigma–Aldrich, and six types of commercial anatase TiO_2 supports were purchased from Millennium Chemical (types (G) and (A)), Ishihara (types (S) and (M)), Hombikat (type (U)) and Sigma–Aldrich (type (A)) and used directly without treatment. The TiO_2 supports were impregnated by excess-solution impregnation using an aqueous $PtCl_4$ solution at the required concentration to obtain 1 wt% Pt. After the solvent was removed at 70 °C by evaporation, the catalysts were dried overnight at 103 °C. The solid was reduced for 3 h in 30% H_2/N_2 gas at 300 °C to eliminate chloride and then calcined in air at 400 °C for 4 h.

2.2. Characterization

The structure of the synthesized materials was examined by X-ray diffraction on a PANalytical X'Pert Pro MPD diffractometer equipped with a Cu-Kα radiation source. Diffraction peaks, which were recorded in the 2θ range between 10° and 80°, were used to identify the structures of the samples. The primary crystallite size of TiO_2 was calculated using the Scherrer equation [14]:

$$d = \frac{0.9\lambda}{B \cos\theta} \quad (4)$$

where λ is the X-ray wavelength that corresponds to Cu-Kα radiation, B is the broadening of the anatase (1 0 1) reflection, and θ is the angle of diffraction that corresponds to the peak broadening.

The specific surface area of the catalysts was measured using an ASAP 2010C (Micromeritics), and the specific surface area was calculated using the BET equation. Each specimen was analyzed after being degassed under vacuum at 110 °C for 3–5 h.

An elementary reaction test was conducted to examine the mechanism of the RWGS reaction. First, the catalysts were purged with Ar at 350 °C for 1 h. After this step, CO_2 and H_2 were supplied in the following order: 10% H_2/Ar → 800 ppm CO_2/Ar. The generated CO and CO_2 were analyzed using a non-dispersion infrared gas analyzer (ZKJ-2, Fuji Electric).

Catalysts were characterized in terms of their dispersion by CO chemisorptions at 25 °C. The catalyst sample, which was activated in a hydrogen (H_2/N_2 = 30/70 as vol.%) flow at 300 °C for 30 min, cooled to 25 °C and then saturated with pulses of CO (CO/He = 10/90 as vol.%).

The Temperature-Programmed Reduction (TPR) using H_2 was measured with 5% H_2/He using 0.3 g of the catalyst at a total flow rate of 50 cc/min. Prior to the H_2 TPR measurements, the catalyst was pretreated in a flow of 5% O_2/He at 300 °C for 1 h and allowed to cool to room temperature. The catalyst was then exposed to dilute hydrogen, and the consumption of hydrogen was monitored using an Autochem 2920 as the temperature was increased to 600 °C at a rate of 10 °C/min.

H_2-Temperature Programmed Desorption (TPD) experiments were performed over prepared catalysts. Approximately 0.3 g of catalyst was reduced in situ with hydrogen at 300 °C. The sample was subsequently purged with Ar at 400 °C to remove adsorbed species from the catalyst surface and then cooled to room temperature under an Ar flow. The catalysts were then exposed to 10% H_2 at 80 °C for 30 min and purged with Ar for 30 min; the desorbed hydrogen was then monitored using a quadrupole mass spectrometer (Pfeiffer Vacuum) by increasing the temperature to 600 °C at a rate of 20 °C/min.

An ICP-atomic emission spectrometer (Perkin-Elmer Optima 3000XL) was used for quantitative analyses. The RF power, plasma flow, coolant flow and nebulizer flow were 1300 W, 15 L/min, 0.5 L/min and 0.8 L/min, respectively. In a Teflon bottle, 0.1 g of the specimen was digested with 2 mL of reagent (HF, HNO_3, and $HClO_4$ 4:4:1, v/v) and then diluted with distilled water. The specimen was finally subjected to ICP analysis. The IC was analyzed using a DIONEX-120 automated dual-column IC. The column was an AS4A SC 4 mm, the flow rate was 1 mL/min, the eluent was 1.8 mM Na_2CO_3/1.7 mM $NaHCO_3$, and the anion self-regenerating suppressor was ASRS-I 4 mm.

Field-emission transmission electron microscopy images were recorded on a JEM-2100F (JEOL) microscope operated at 200 kV. Samples for FE-TEM measurements were prepared by suspending ultrasonically treated catalyst powder in ethanol and placing a drop of the suspension on a Cu grid.

2.3. Catalytic activity tests

The RWGS reaction was performed in a fixed-bed flow reactor. In the feed section, the reactants were passed through a set of MKS 1179A mass flow controllers. An undiluted gaseous mixture was used in these experiments. A quartz reactor (10 mm ID), which was heated using a furnace with three independent heating zones, was used, and each zone was controlled with a proportional-integral-derivative (PID) temperature controller, which facilitated isothermal operation. The temperature profile along the bed was measured using a K-type thermocouple that was located at the central axis of the reactor. The reaction temperature was varied between 300 and 600 °C. A H_2/CO_2 gaseous mixture was introduced into the catalyst bed at a total flow rate of 100 mL/min. For these experiments, 0.5 g of the catalyst was loaded into the reactor.

Reaction rates were measured in separate experiments, in which the conversion of reactants was maintained below 10% such that differential reaction conditions and negligible heat and

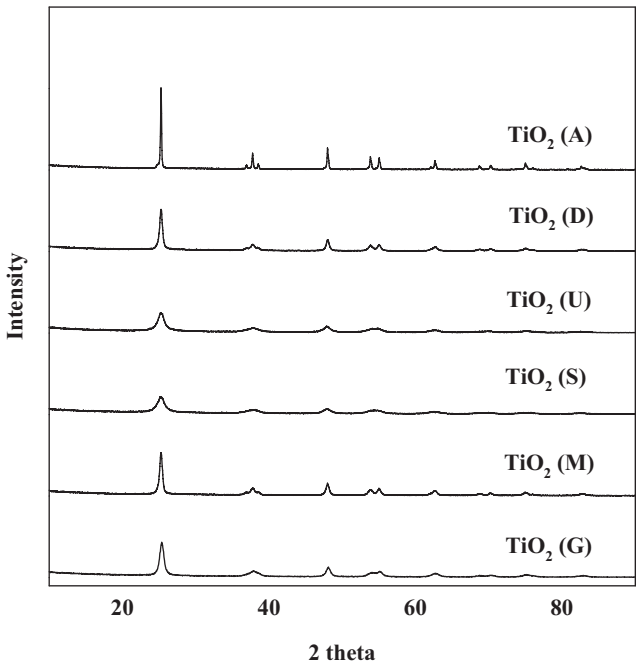

Fig. 1. XRD patterns of the TiO_2 supports.

mass-transfer effects could be assumed. Rates were calculated using the following expression,

$$r = \frac{X * F_{CO_2}}{W} \quad (5)$$

where r is the reaction rate of CO_2 (mol s^{-1} g^{-1} cat), F_{CO_2} is the total flow rate (mol s^{-1}), W is the mass of catalyst (g), and X is the conversion of CO_2, respectively. These results, along with the metal dispersion measurements, were used to calculate the turnover frequency (TOF) of CO_2, which is defined as the moles of CO_2 converted per surface metal atom per second (s^{-1}):

$$\mathrm{TOF} = \frac{r_{CO_2} * \mathrm{AB_M}}{D * X_M} \quad (6)$$

where AB_M represents the atomic weight of metal M, X_M is the metal content (g_{met}/g_{cat}), and D is the metal dispersion [13].

3. Results and discussion

3.1. Physicochemical characteristics of the TiO_2 support and catalysts

Fig. 1 shows the XRD patterns of the as-received TiO_2 support, and all samples consisted of anatase-phase TiO_2. As shown Table 1, the primary crystallite size of the TiO_2 samples, which was calculated based on the XRD peak broadening and the BET surface area of TiO_2, varied. The primary crystallite size of TiO_2 increased as the BET surface area decreased, which indicates that the porosity of TiO_2 was dependent on the primary crystallite size.

The diffractograms of fresh and conditioned Pt/TiO_2 catalysts prepared with 6 types of TiO_2 are shown in Fig. 2. All samples were anatase-phase TiO_2, and the crystallinity of the TiO_2 was observed to decrease in the Pt-impregnated catalysts. BET measurements showed that the Pt deposition induced a decrease in the surface area (Table 1). The conditioned catalysts also exhibited lower surface areas and larger TiO_2 crystallite sizes, which were believed to be due to the heat effect during the catalyst preparation process and during the activity tests. There are two potential reasons why the SSA was more severely decreased at TiO_2, which has a high specific surface area. First, when Pt is deposited on each TiO_2 support under the same conditions, the dispersion of Pt will differ depending on the difference in the specific surface area of the TiO_2 supports. Such a difference in the dispersion will affect metal–metal agglomeration because the well-dispersed Pt sites can easily cause agglomeration. Second, the SSA is affected by the unique manufacturing conditions of the TiO_2 supports. Because the TiO_2 supports used in this study were manufactured under different conditions by the different manufacturers, TiO_2 supports exhibit unique characteristics. These different conditions (especially the thermal treatment temperature) can influence the thermal stability of the TiO_2 supports. In the case of TiO_2 (D) and TiO_2 (M), the specific surface areas of the TiO_2 and Pt/TiO_2 can differ.

Table 1
Phase composition, primary crystallite size and specific surface area of TiO_2 supports and Pt/TiO_2 catalysts.

TiO_2 supports	Phase	Primary crystallite size (nm)		Specific surface area (m^2/g)
TiO_2 (A)	Anatase	41.9		11
TiO_2 (D)	Anatase	20.6		77
TiO_2 (G)	Anatase	11.4		220
TiO_2 (M)	Anatase	15.6		97
TiO_2 (S)	Anatase	8.5		276
TiO_2 (U)	Anatase	8.6		288
Catalysts	Phase	Primary crystallite size (nm)		Specific surface area (m^2/g)
		Fresh one	Conditioned one	
Pt/TiO_2 (A)	Anatase	48	50	9
Pt/TiO_2 (D)	Anatase	22	26	36
Pt/TiO_2 (G)	Anatase	12	19	52
Pt/TiO_2 (M)	Anatase	18	29	24
Pt/TiO_2 (S)	Anatase	14	22	56
Pt/TiO_2 (U)	Anatase	14	21	56

The physicochemical characteristics of the various TiO_2-supported Pt catalysts synthesized in the present study are summarized in Table 2. As shown in Table 2, the dispersion of Pt in the catalysts was significantly different. The TiO_2 supports in the Pt/TiO_2 catalysts used in this study have different properties (e.g., specific surface area, pore structure, and thermal stability), and these different properties of the TiO_2 supports may produce different agglomeration effects, which would affect the dispersion of Pt on the catalysts.

3.2. Activities of the Pt/TiO_2 catalysts

The activities of the various Pt/TiO_2 catalysts are presented in Fig. 3. The equilibrium conversion, which is predicted by thermodynamics, is also shown for comparison. The activity increased as the reaction temperature was increased. The Pt/TiO_2 (G) catalyst showed the highest catalytic activity, which was similar to the

Table 2
Physicochemical characteristics of Pt/TiO_2 catalysts and their reaction rate for RWGS reaction.

Catalysts	Metal contents[a] (wt%)	Metal dispersion (%)	Reaction rate at 300 °C (mol s^{-1} g^{-1} cat)
Pt/TiO_2 (A)	0.98	0.3	2.03×10^{-3}
Pt/TiO_2 (D)	0.97	21.1	2.90×10^{-3}
Pt/TiO_2 (G)	0.99	18.2	6.48×10^{-3}
Pt/TiO_2 (M)	0.99	5.6	4.25×10^{-3}
Pt/TiO_2 (S)	0.97	4.6	6.25×10^{-3}
Pt/TiO_2 (U)	0.98	42.1	5.55×10^{-3}

[a] A value by IC & ICP analysis.

Table 3
Pt dispersion and TOFs of various Pt/TiO_2 catalysts.

Catalysts	Notation	Pt dispersion (%)	TOFs at 300 °C ($mol\,s^{-1}$)
1% Pt/TiO_2 (G) pretreated at 400 °C	PT 400	18.2	0.429
1% Pt/TiO_2 (G) pretreated at 650 °C	PT 650	1.2	2.716
0.1% Pt/TiO_2 (G) pretreated at 400 °C	0.1 PT 400	42.2	0.423
0.5% Pt/TiO_2 (G) pretreated at 400 °C	0.5 PT 400	26.0	0.428
1% Pt/TiO_2 (G) pretreated at 400 °C	1 PT 400	18.2	0.429
3% Pt/TiO_2 (G) pretreated at 400 °C	3 PT 400	9.0	0.425

results based on CO_2 conversion with equilibrium conversion at all of the investigated reaction temperatures. The Pt/TiO_2 (A) and (D) catalysts were significantly less active than the other catalysts examined.

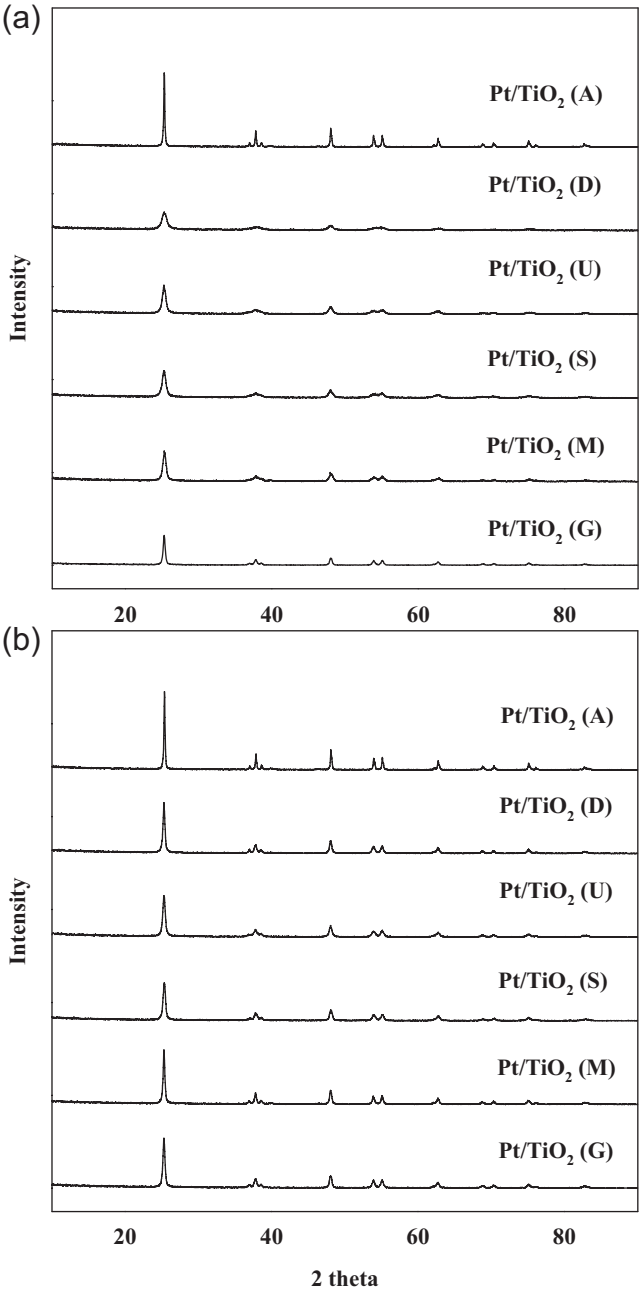

Fig. 2. XRD patterns of the Pt/TiO_2 catalysts (a) and Pt/TiO_2 catalysts after the activity test (b).

Before investigating the reason for this difference in activity, we first evaluated the positions of the active sites. In general, the activity of Pt catalysts can be compared in terms of their TOFs, and these comparisons can be used to assess whether the activity is determined by dispersion or by the intensity of the active site. This rationale is valid if the active site of the catalyst is confined only to Pt. If the reaction occurs in the support, the compared activity in terms of TOF is meaningless. Catalysts used in this study contained Pt as the active metal. Thus, the position of the main active site (support or active metal or both) should be assessed to express the activity of the catalyst in terms of TOF. The catalysts were prepared at different calcination temperatures to examine the active position of the Pt/TiO_2 catalysts, and their physicochemical characteristics are presented in Table 3. The conversion used to calculate the reaction rates and TOFs was maintained at less than 10% to eliminate effects caused by mass transfer. Interestingly, the Pt/TiO_2 650 and Pt/TiO_2 400 catalysts were shown to exhibit different TOFs. TEM analyses were performed to investigate the morphology of Pt; the results are shown in Fig. 4. The Pt/TiO_2 400 catalyst had a mean Pt size of approximately 2.5 nm, and the mean Pt size increased by several tens of nm due to the agglomeration effect. The dispersion of Pt is believed to be lower in the Pt/TiO_2 650 catalyst than in the Pt/TiO_2 400 catalyst.

According to the TEM results in Fig. 4, the difference in the TOF between the two catalysts can be attributed to the structure-sensitive characteristics of Pt. To better understand the impact of the morphological characteristics of Pt on catalytic activity, the activity of the catalysts at different Pt concentrations (0.1–3%) was measured (Table 3). The conversion rate was maintained at less than 10% because the reaction rate of the catalyst depends on the calcination temperature and TOF. In this analysis, the TOFs of all catalysts were approximately the same. This result implies that the structural characteristics of the Pt in the Pt/TiO_2 catalyst are "insensitive" in the RWGS reaction.

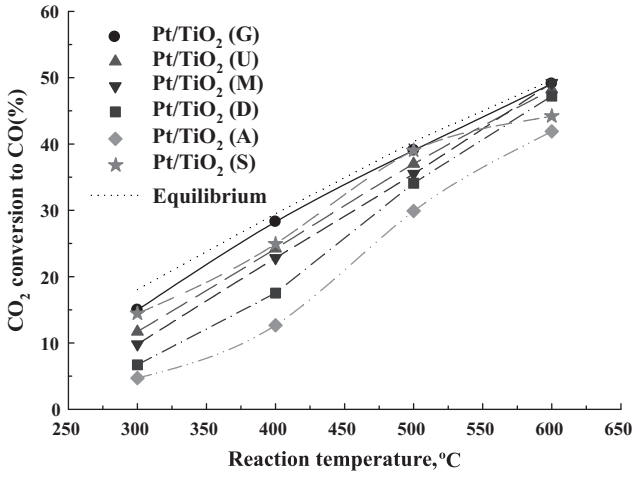

Fig. 3. Activities in the RWGS reaction over Pt/TiO_2 catalysts.

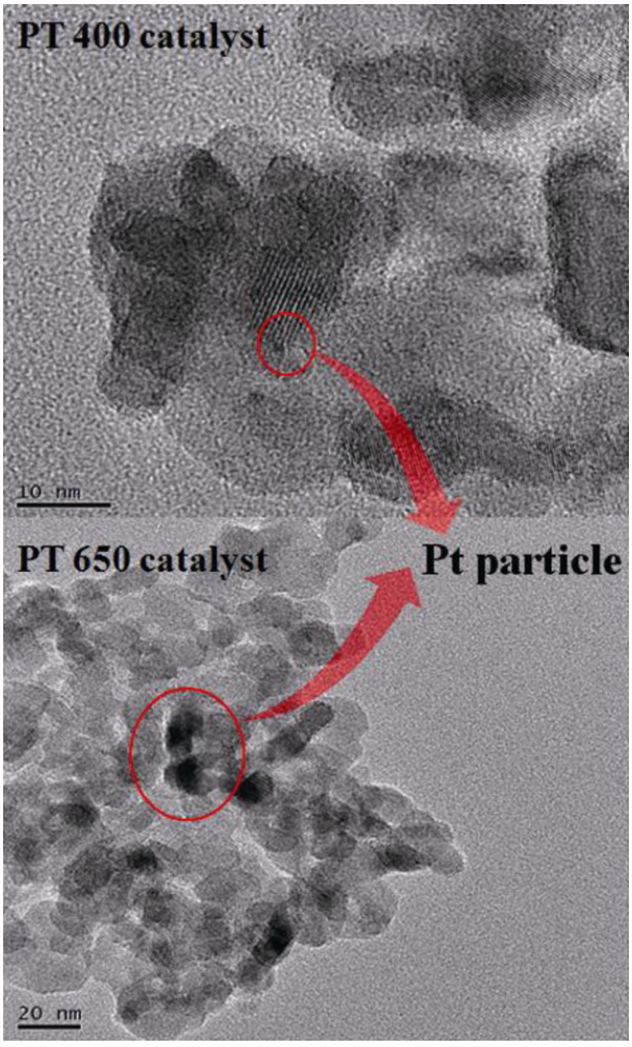

Fig. 4. FE-TEM images of Pt/TiO_2 catalysts calcined at different temperatures.

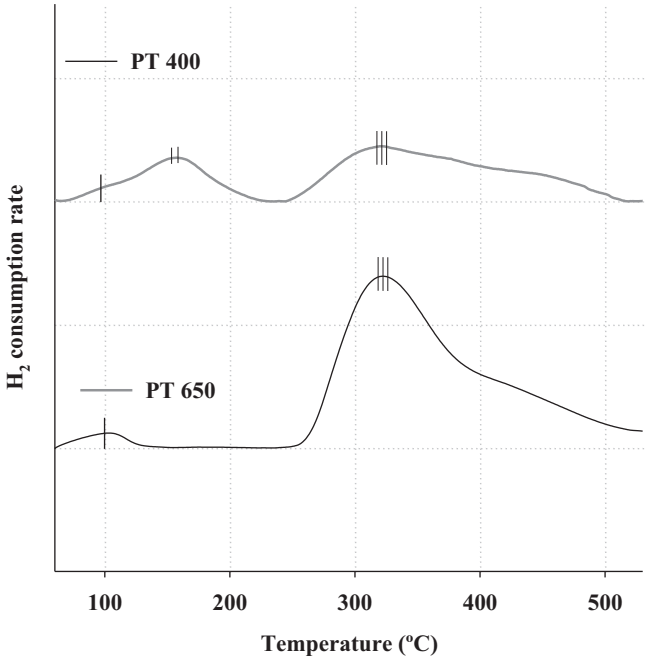

Fig. 5. H_2 TPR profiles of Pt/TiO_2 catalysts calcined at different temperatures.

Table 4
The information of first peak in H_2 TPR profiles over Pt/TiO_2 catalysts.

Catalysts	Peak position (°C)	Hydrogen uptake rate (mmol)
Pt/TiO_2 (A)	154	0.186
Pt/TiO_2 (D)	146	1.378
Pt/TiO_2 (G)	118	0.407
Pt/TiO_2 (M)	110	0.436
Pt/TiO_2 (S)	116	0.288
Pt/TiO_2 (U)	112	1.082

Three peaks were observed in the H_2 TPR profiles (Fig. 5). The first peak corresponded to the reduction of the Pt oxide species, and the second peak corresponded to the reduction of TiO_2, which interacts strongly with Pt, located at an adjacent Pt. The third peak represents the reduction of surface TiO_2 particles. In the case of the third peak, Pt-supported catalysts are known to be formed at temperatures less than that where pure TiO_2 is formed. This phenomenon was clearly observed in the TPR profiles of not only the catalysts that incorporated Pt but also those that incorporated other noble metals and reducible supports [15]. This behavior can be explained by the hydrogen spillover effect, which occurs from the metallic Pt. As shown in Fig. 5, the first peak where PtO_2 and PtO were reduced showed a similar pattern. In addition, the third peak, which was caused by the spillover effect, appears at almost the same position. The spillover effect occurred because the reducible surfaces TiO_2 sites were reduced by activated H atoms. Thus, the Pt sites of the Pt/TiO_2 400 and Pt/TiO_2 650 catalysts must exhibit similar H_2 dissociation properties. However, the second peak, which is related to the SMSI effect, was not observed for the Pt/TiO_2 650 catalyst. The second peak corresponds to a new active site ($Pt–O_v–Ti^{3+}$) formed by the migration of electrons to Pt. This migration was caused by the strong interaction of Pt with reduced Ti^{3+} sites, and Pt provides an oxygen-binding site to TiO_2. Therefore, the absence of the second peak in the TPR profile implies that the Pt/TiO_2 650 catalyst could not provide a Ti site for oxygen binding, which is contrary to the case for the Pt/TiO_2 400 catalyst.

These combined results imply that Pt is not the main active site in the RWGS reaction, i.e., the Pt sites in the Pt/TiO_2 650 catalyst do not have superior activity compared with the Pt sites in the Pt/TiO_2 400 catalyst, but rather, the Pt/TiO_2 400 catalyst contains more active Ti sites. Therefore, a comparison of activity in terms of TOFs, which only considers the number of Pt sites, is meaningless, and the number of Ti sites that participated in the reaction was a more important factor.

3.3. *Reducibility and adsorption characteristics of H_2 and CO_2 on the Pt/TiO_2 catalysts*

The hydrogen consumption profiles of the Pt/TiO_2 catalysts with different types of TiO_2 supports were obtained from the TPR experiments (Fig. 6). As shown in Fig. 6, the peaks where PtO_2 and PtO were reduced to Pt were in similar positions, except in the case of the Pt/TiO_2 (D) catalyst. As previously discussed, because the main active site where the RWGS reaction occurs is not on Pt, no specific correlation may exist between the structure of Pt or the number of sites that can be reduced and the activity. In the TPR profiles of the various Pt/TiO_2 catalysts shown in Table 4, the hydrogen consumption (mole) corresponds to the first peak. Based on this analysis, a moderate correlation with Pt dispersion was observed. In addition, the location of the first peak can be used as a measure of the energy (temperature) of the Pt sites of the catalyst surface that are reduced to metallic Pt. This difference is caused by structural differences, such as the degree of agglomeration of the active metal [16,17]. As expected, the position and area of the first peak was not correlated

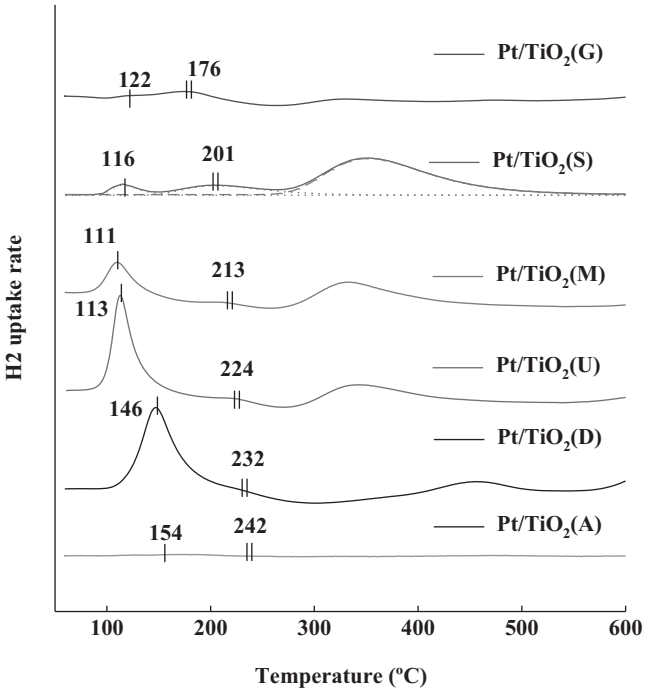

Fig. 6. H_2 TPR profiles of various Pt/TiO_2 catalysts.

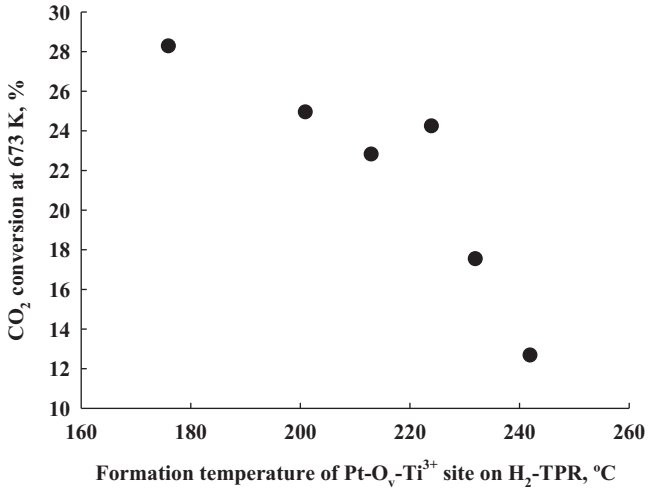

Fig. 7. The correlation between the activity and formation temperature of the $Pt–O_v–Ti^{3+}$ sites.

with the activity of the catalysts. Goguet et al. [11] have reported that the main intermediate in the RWGS reaction in the presence of a Pt/CeO_2 catalyst was the carbonate species, which were formed on the CeO_2 site bound to oxygen. This result implies that the redox properties of the support are more important than the structure or dispersion of Pt sites. The second and third peaks are related to the redox properties of TiO_2 in the TPR profile. The third peak for the catalysts, with the exception of the Pt/TiO_2 (D) catalyst, was located in approximately the same position, i.e., these results imply that all catalysts except Pt/TiO_2 (D) have approximately the same properties with respect to the spillover effect. The position of the first peak can represent the structure-sensitivity of the active Pt sites. For these reasons, the third position in the TPR peak is thought to be closely correlated with the position of the first peak. In contrast, the position of the second peak for each catalyst varied. The second peak for the Pt/TiO_2 (G) catalyst was observed at approximately 120 °C and 200 °C for the Pt/TiO_2 (M) catalyst. This result implies that the activation energy required to form new active sites for each TiO_2 specimen was different.

The origin of the difference in activation energy required for the formation of the $Pt–O_v–Ti^{3+}$ sites should be discussed. As shown in Fig. 7, the temperature at which the $Pt–O_v–Ti^{3+}$ sites are formed was highly correlated with catalytic activity. These differences in activation energy difference were thought to be caused by the structure sensitivity problems of the Pt sites for each catalyst and the differences in the reproducibility of the TiO_2 samples. However, based on the location of the first and third peaks in the H_2 TPR of the Pt/TiO_2 catalysts, little structural difference was observed between the Pt sites. In general, noble metals, such as Pt, Ru, and Pd, are not expected to interact strongly with stoichiometric TiO_2 [18]. Dispersed noble-metal crystallites are well known to interact with partially reduced TiO_2 supports. Therefore, the formation of $Pt–O_v–Ti^{3+}$ sites may depend on the specific reduction temperature at Ti sites located adjacent to Pt sites, i.e., these findings suggest that the temperature at which TiO_2 can be reduced in part by H_2 molecules can determine the temperature necessary to form $Pt–O_v–Ti^{3+}$ sites. Thus, the formation of $Pt–O_v–Ti^{3+}$ sites in the TPR profiles of Pt/TiO_2 650 and 400 catalysts in the previous section was not observed at the Pt/TiO_2 650 catalyst because of a deficiency in the reducibility of Ti sites adjacent to Pt sites. A significant difference in the TiO_2 crystallite size was observed in the XRD analyses of the two catalysts (data not shown). TiO_2-specific reducibility will be discussed in more detail in the subsequent paragraphs.

Because the presence of $Pt–O_v–Ti^{3+}$ sites on the Pt/TiO_2 catalysts increases the electron-donating ability of the materials, the electron density on the surface of the catalyst will change. In addition, when an electron is moved from CO to an unoccupied d orbital of a metal, a covalent bond between the two atoms is formed. If the electron density of the metal is high, the electron donation from the highest occupied molecular orbitals (HOMOs) of CO to the metal (σ-bond) is decreased, which results in a hindrance of CO adsorption. Therefore, the electron density on the surface of the catalyst may be an important factor in the RWGS reaction. According to Panagiotopoulou and Kondarides [7], H_2 TPD is an effective method for investigating the electron-donating abilities of Pt and $Pt–O_v–Ti^{3+}$ sites based on the desorption behavior of the adsorbed H_2. Thus, H_2 TPD analysis was conducted to examine the electron-donating ability of each catalyst (Fig. 8).

Peaks generated for all catalysts were largely divided into the three categories. The LT (low-temperature) peak was formed at approximately 110 °C, the MT (medium-temperature) peak was formed at approximately 200 °C, and the HT (high-temperature) peak was formed at approximately 360 °C.

With the exception of the Pt/TiO_2 (D) catalyst, the LT peak was different for each catalyst, but all were similar with respect to their position. The results of the TPR (Fig. 6) were similar, which indicates that no correlation with the activities of the catalysts was observed. However, the LT peak did effect the position of the HT peak. The HT peak positions of catalysts that exhibited a high LT peak shifted toward lower temperatures relative to the other catalysts. The HT peak has been shown to be associated with the spillover effect of the support [19,20]. In the TPR analysis (Fig. 6), the spillover effect of all catalysts, except that of Pt/TiO_2 (D), was almost identical. These results imply that the spillover effect was different between the TPR and TPD experiments. In the H_2 TPD experiments, only the spillover effect due to desorbed H_2 was observed. In contrast, in the H_2 TPR experiment, the amount of dissociated H atoms did not result in the spillover effect because hydrogen was continuously infused. Thus, the spillover effect for each catalyst was different.

Unlike the LT and HT peaks, the MT peaks exhibited independent properties. For all of the catalysts, the position of the MT peak was observed to be independent of the positions of the LT and HT

Table 5
The position of second peak in H_2 TPR profiles and generated CO moles from elementary reaction test.

Catalysts	Peak position (°C)	Dispersed Pt moles on catalyst surface (μmol)	CO moles (μmol)	CO–Pt
Pt/TiO_2 (A)	242	0.18	3.18	12.66
Pt/TiO_2 (D)	232	10.83	26.61	17.52
Pt/TiO_2 (G)	176	9.33	63.23	28.26
Pt/TiO_2 (M)	213	2.86	32.25	22.80
Pt/TiO_2 (S)	201	2.37	40.83	24.93
Pt/TiO_2 (U)	224	21.62	51.78	24.22

peaks. Interestingly, this position was found to be associated with the temperature at which the TPR Pt–O_v–Ti^{3+} sites were formed (Table 5). According to Panagiotopoulou and Kondarides [7], the MT H_2 peak is associated with the desorption of H_2 adsorbed on the Pt–TiO_2 interface site. They also reported that the MT peak of the Pt/TiO_2 catalysts that contain alkali metals shifted to a lower temperature than that of pure Pt/TiO_2, which was caused by an increase in the electron density of Pt due to the presence of the electropositive alkali metal (because Pt–O_v–Ti^{3+} sites are formed in the case of pure Pt/TiO_2, an MT peak is observed). Thus, the fact that the MT peak for each catalyst was observed at a different position in this study implies that the electron density of the catalytic surface of Pt–O_v–Ti^{3+} site varied for each catalyst. As the electron density of Pt in the catalyst increases, the adsorption of H_2 becomes more difficult, and H_2 is desorbed at low temperatures. However, unlike the study by Panagiotopoulou and Kondarides [7], no alkali addition was used in this study. Nevertheless, the difference in the positions of MT peaks was caused by differences in the nature of the Pt/TiO_2 interfacial sites. In the Pt site of the Pt–O_v–Ti^{3+} sites, the electron density increases due to the electron-transfer effect of the Ti site. The Pt/TiO_2 catalysts used in this study required

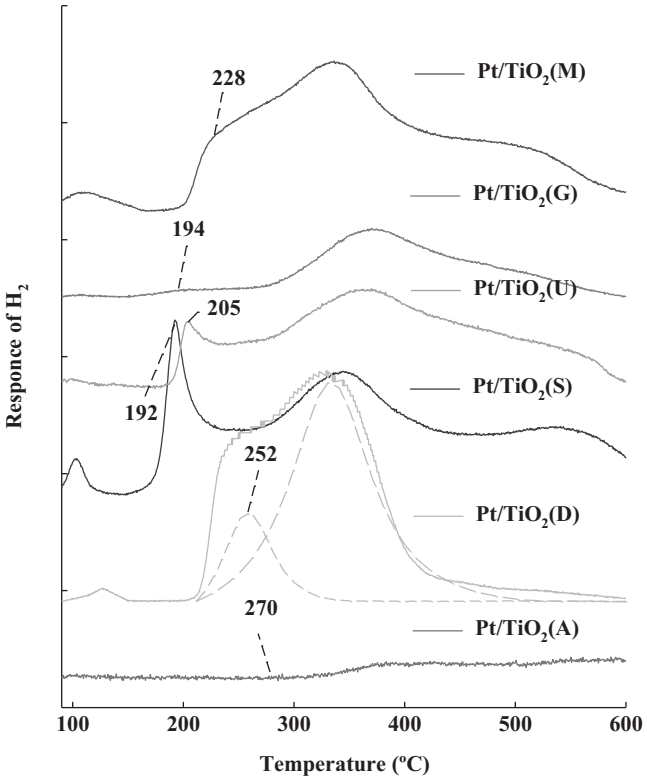

Fig. 8. H_2 TPD profiles of various Pt/TiO_2 catalysts.

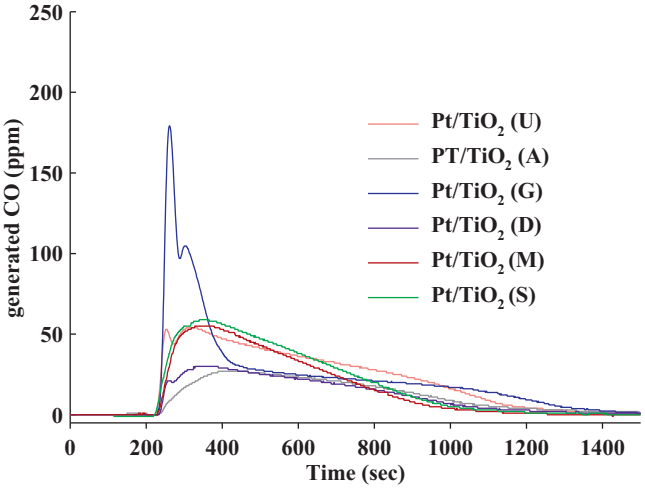

Fig. 9. Elementary reaction tests of various Pt/TiO_2 catalysts.

different temperatures to form Pt–O_v–Ti^{3+} sites. The Pt–O_v–Ti^{3+} sites formed at lower temperatures compared with the other catalysts. This result implies that the Ti sites are easily reducible. This phenomenon suggests that the degree of reduction of TiO_2 can vary even by the same hydrogen, and the electron-donating ability of the Pt site can be changed. Therefore, the TiO_2-specific reducibility can affect the temperature at which Pt–O_v–Ti^{3+} sites are formed, and the electron-donating ability of the Pt–TiO_2 at the interface sites can therefore be altered.

According to the TPR and TPD results, the Pt sites, as well as the active sites of the support, are important to the activity of Pt/TiO_2 catalysts.

3.4. Active sites on the TiO_2 supports and their controlling factor

Goguet et al. [11] claimed that carbonate formed at oxygen-vacant sites of the support was the main intermediate of the reaction and reported the importance of the redox characteristics of the support. The results of the H_2 TPR and TPD experiments confirmed that the reducibility of TiO_2 is an important factor with respect to the catalytic activity. These results also imply that sites where the reaction on the support can occur are present. Elementary reaction tests using the Pt/TiO_2 catalysts were performed (Fig. 9) to quantitatively investigate whether the reaction occurs at the TiO_2 sites on the support. The elementary reaction test was used to quantify the generation of CO upon injection of a low concentration of CO_2 after the catalyst was pretreated with hydrogen (i.e., oxygen-vacant sites were formed on the catalyst). At this point, the oxygen-vacant site of the Pt/TiO_2 catalyst can be formed at the Pt and TiO_2 sites. In addition, according to Goguet et al. [11], the intermediates of the RWGS reaction, which can be formed on the surface of the catalyst, include carbonyl species bound to Pt and carbonate and formate species formed on the support. Unless the RWGS reaction on the TiO_2 site proceeds, only Pt-carbonyl species can be formed on the surface, and the number of Pt-carbonyl species cannot exceed the theoretical number of Pt sites, which was calculated based on the Pt dispersion on the surface of the catalyst. Therefore, theoretically, only 1 mol of CO per 1 mol of Pt can be adsorbed.

CO was shown to be generated after a certain amount of time, irrespective of the catalyst type, when the pretreated catalyst was exposed to CO_2 (Fig. 9). However, the amount of CO generated varied for each catalyst, and the linear relationship with the activity of the catalyst is shown in Fig. 10. The amount of CO generated on the surface of the catalyst and CO/Pt ratio is shown in Table 5. All

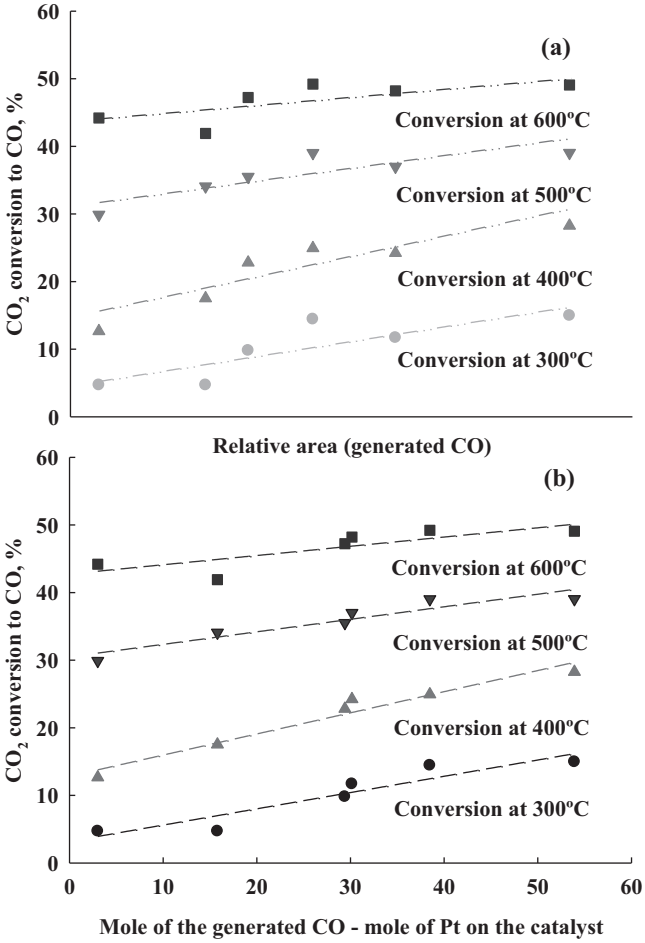

Fig. 10. Effect of active TiO_2 sites on the CO_2 conversion in the RWGS reaction over Pt/TiO_2 catalysts. (a) The correlation between the catalytic activity and the active site ($Pt+TiO_2$ site) on the catalyst. (b) The correlation between the catalytic activity and the active site (only active TiO_2 site) on the catalyst.

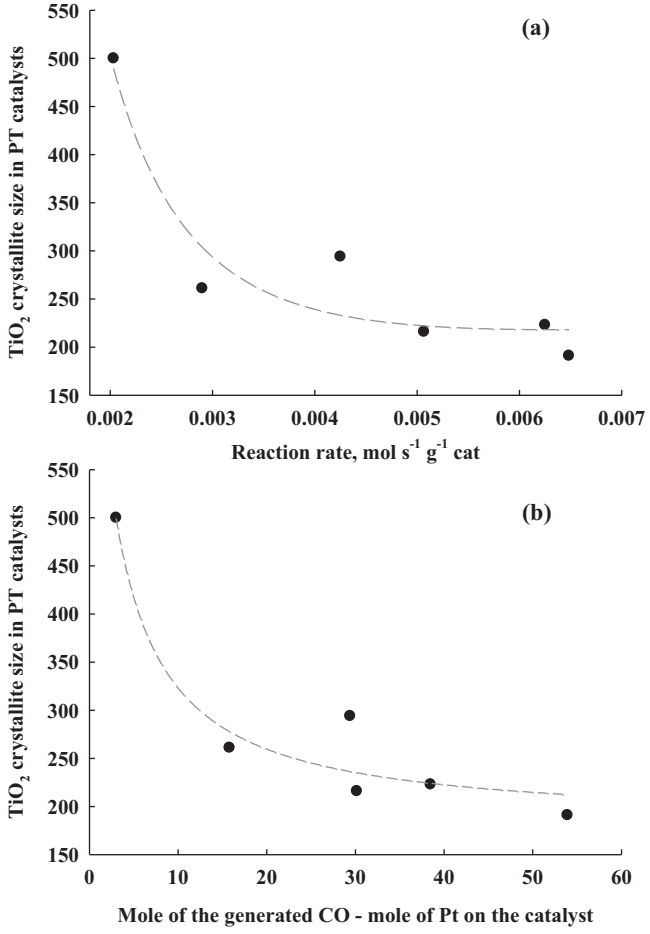

Fig. 11. (a) Effect of primary crystallite size of TiO_2 support on the activity of TiO_2 sites. (b) Correlation between the number of active TiO_2 sites and the TiO_2 crystallite size.

of the catalysts used in this study exhibited a CO/Pt ratio greater than 1, and the values were different for each catalyst. As previously mentioned, a CO/Pt ratio that exceeds 1 indicates that the reaction proceeded at TiO_2 sites instead of Pt sites. As shown in Fig. 10(b), the relationship between the activity of the catalyst and the moles of CO formed at the TiO_2 sites was linear. Fig. 10(a) shows the relationship between Pt dispersed in the catalyst and the TiO_2 sites, and Fig. 10(b) shows the data when only the TiO_2 sites are considered. According to the TPR results (Fig. 6) and the results of Goguet et al. [11], TiO_2 sites participate in reactions that involve oxidation and reduction. Because these redox properties varied for each TiO_2 sample, the samples would exhibit different reaction activities. Of course, the dispersion of Pt can strongly influence the activity of the catalyst. However, as shown in Table 5, the CO/Pt ratio was greater than 1. Therefore, because the reaction activities of the catalysts used in this study were strongly affected by the number of TiO_2 sites with redox properties rather than by Pt dispersion, the factors that affect the redox properties of TiO_2 need to be examined.

Panagiotopoulou and Kondarides [8] have reported that the activity of Pt/TiO_2 catalysts with various properties during the WGS reaction is affected by the primary crystallite size of TiO_2. In addition, Jacobs et al. [21] have reported that the support was reduced in reactions that involved a Pt/CeO_2 catalyst as the size of CeO_2 crystallites was increased. These previous studies imply that smaller-sized supports exhibit better redox properties, which may also affect activity. Therefore, the effect of the morphological characteristics of the TiO_2 support on catalytic activity was investigated (Table 2), and the relationship between the activity and crystallite sizes of the Pt/TiO_2 catalysts are shown in Fig. 11. In this analysis, only the sizes of the TiO_2 crystallites after the reaction test were evaluated because its size can be changed by the reaction. As shown in Fig. 11, the TiO_2 crystallite size was strongly correlated with the activity of the Pt/TiO_2 catalyst. As the crystallite size of TiO_2 was increased, the reaction activity dramatically decreased. The curve exhibits an exponential shape because of the relationship between crystallite size and surface area/unit volume. The decrease in reaction activity was accompanied by a substantial reduction in the redox properties of the TiO_2 support. In addition, based on these results and on the previous discussion of previously published findings, the smaller TiO_2 crystallites possibly result in larger Pt/TiO_2 interfaces, which lead to an increase in the number of reducible active sites.

These results are consistent with those of Panagiotopoulou and Kondarides [8] and Bunluesin et al. [22], both of whom studied the effects of support size on the WGS reaction. The mechanism of the WGS reaction is generally divided into the regenerative mechanism and the associative mechanism. Panagiotopoulou and Kondarides [8] and Bunluesin et al. [22] claimed that, because the reducibility of their supports was excellent, the reaction activity was superior based on the regenerative mechanism. Goguet et al. [11] reported that the mechanism of the RWGS reaction can be described by the RWGS redox reaction (regenerative mechanism) and that the main pathway was the formation of carbonate species due to the redox properties of the support. TPR and elementary reaction tests, as

well as the TiO_2 crystallite size, all demonstrated that the TiO_2 sites could function as an active site in the RWGS reaction and that this effect relied on TiO_2-specific reducibility. Thus, it is thought that the regenerative mechanism that is affected by the reducibility of TiO_2 in the RWGS reaction using the Pt/TiO_2 catalyst can be applied and that this reducibility is highly dependent on the crystallite size of TiO_2.

4. Conclusions

Pt/TiO_2 catalysts with various types of TiO_2 were prepared using the impregnation method, and their physicochemical properties were investigated. The activity of 6 types of Pt/TiO_2 catalysts in the reverse water–gas shift reaction varied. Because TiO_2 sites also acted as active sites, the activity in terms of TOFs was meaningless. The H_2 TPR and H_2 TPD analyses confirmed the generation of a new active site, which was $Pt–O_v–Ti^{3+}$, in the Pt/TiO_2 catalysts, and its activity was dependent on the reducibility of the TiO_2 supports. The primary crystallite size calculated by XRD analysis indicated that the TiO_2 crystallite size was the key factor that dictates the reducibility of TiO_2 sites. Therefore, we concluded that the catalytic activity of Pt/TiO_2 in the reverse water–gas shift reaction was affected to a greater extent by the properties of the TiO_2 supports than by the structure of the Pt.

References

[1] J. Ma, N. Sun, X. Zhang, N. Zhao, F. Xiao, W. Wei, Y. Sun, Catal. Today 148 (2009) 221–231.
[2] W. Wang, S. Wang, X. Ma, J. Gong, Chem. Soc. Rev. 40 (2011) 3703–3727.
[3] S.W. Park, O.S. Joo, K.D. Jung, H. Kim, S.H. Han, Appl. Catal. A 211 (2001) 81–90.
[4] C.S. Chen, W.H. Cheng, S.S. Lin, Appl. Catal. A 257 (2004) 97–106.
[5] W. Luhui, Z. Shaoxing, L. Yuan, J. Rare Earths 26 (2008) 66–70.
[6] Y. Liu, D.Z. Liu, Int. J. Hydrogen Energy 24 (1999) 351–354.
[7] P. Panagiotopoulou, D.I. Kondarides, J. Catal. 267 (2009) 57–66.
[8] P. Panagiotopoulou, D.I. Kondarides, J. Catal. 225 (2004) 327–336.
[9] P. Panagiotopoulou, D.I. Kondarides, Catal. Today 127 (2007) 319–329.
[10] P. Panagiotopoulou, D.I. Kondarides, Catal. Today 112 (2006) 49–52.
[11] A. Goguet, F.C. Meunier, D. Tibiletti, J.P. Breen, R. Burch, J. Phys. Chem. B 108 (2004) 20240–20246.
[12] G. Pekridis, K. Kalimeri, N. Kaklidis, E. Vakouftsi, E.F. Iliopoulou, C. Athanasiou, G.E. Marnellos, Catal. Today 127 (2007) 337–346.
[13] S.S. Kim, K.H. Park, S.C. Hong, Appl. Catal. A 398 (2011) 96–103.
[14] B.D. Cullity, Elements of X-ray Diffraction, Addison-Wesley, Reading, MA, 1978.
[15] S.S. Kim, S.J. Lee, S.C. Hong, Chem. Eng. J. 169 (2011) 173–179.
[16] K.-P. Yu, W.-Y. Yu, M.-C. Kuo, Y.-C. Liou, S.-H. Chien, Appl. Catal. B 84 (2008) 112–118.
[17] Q. Wang, G. Li, B. Zhao, M. Shen, R. Zhou, Appl. Catal. B 101 (2010) 150–159.
[18] U. Diebold, Surf. Sci. Rep. 48 (2003) 53–229.
[19] P.G. Menon, G.F. Froment, J. Catal. 59 (1979) 138–147.
[20] J.T. Miller, B.L. Meyers, F.S. Modica, G.S. Lane, M. Vaarkamp, D.C. Koningsberger, J. Catal. 143 (1993) 395–408.
[21] G. Jacobs, L. Williams, U. Graham, G.A. Thomas, D.E. Sparks, B.H. Davis, Appl. Catal. A 252 (2003) 107–118.
[22] T. Bunluesin, R.J. Gorte, G.W. Graham, Appl. Catal. B 15 (1998) 107–114.